*Korean J. Chem. Eng.*, 37(11), 2011-2019 (2020)
DOI: 10.1007/s11814-020-0618-y

pISSN: 0256-1115
eISSN: 1975-7220

# A new approach to tailoring the separation characteristics of polyethersulfone nanofiltration membranes by 8-hydroxyquinoline functionalized $Fe_3O_4$ nanoparticles

**Saeed Ansari, Abdolreza Moghadassi†, and Sayed Mohsen Hosseini†**

Department of Chemical Engineering, Faculty of Engineering, Arak University, Arak 38156-8-8349, Iran
(*Received 14 February 2020 • Revised 5 June 2020 • Accepted 30 June 2020*)

**Abstract**−8-Hydroxyquinoline (8-HQ) was used for modification of $Fe_3O_4$ nanoparticles (NPs) and preparation of polyethersulfone (PES)-based mixed matrix membranes (MMMs) by phase inversion process. The synthesized nanoparticles were characterized by Fourier transform infrared spectroscopy (FTIR), Energy dispersive x-ray spectroscopy (EDX), and Field emission scanning electron microscopy (FESEM). The effect of different concentrations of 8-HQ/$Fe_3O_4$ NPs into the PES as membrane matrix was investigated by FESEM and atomic force microscopy (AFM). The performance of prepared membranes was evaluated by the water contact angle, pure water flux (PWF), porosity, means pore size, and salt rejection. Bovine serum albumin (BSA) solution was used to investigate the antifouling properties of fabricated membranes. The results showed a decreasing water contact angle from 68.1° for the pristine membrane to 38.3° for M5 at 0.5 wt% 8-HQ/$Fe_3O_4$ NPs. The PWF enhanced for all mixed matrix membranes compared with the pristine membrane. The highest PWF (21.5 L/m$^2$h) was measured for M4 at 0.2 wt% NPs, Wwhile it was 7.1 L/m$^2$h for pristine membrane. Salt rejection improved from 58.55% in M1 (pristine membrane) to 96% in M4 (at 0.2 wt% of 8-HQ/$Fe_3O_4$ NPs). Also, the modified membranes showed suitable antifouling property.

Keywords: Nanofiltration Membrane, $Fe_3O_4$ Nanoparticles, 8-Hydroxyquinoline, Functionalized NPs, Improved Separation Characteristics

## INTRODUCTION

Nanofiltration (NF) has drawn great attention for wastewater treatment because of low cost, low operating pressure, easy to fabrication. NF membranes with a molecular weight cut-off of 200-1,000 g mol$^{-1}$ can separate divalent ions by different mechanisms, such as size exclusion and charge effects. Therefore, the development of high-efficiency NF membranes for achievement to the trade-off between permeability and selectivity and excellent antifouling properties has been the focus studies [1-6]. The use of nano-scale molecules enhances the unique physical properties [7-9]. Hybrid materials in the preparation of membrane improve chemical stability and mechanical strength due to the presence of nanoparticles. The successful application of nanocomposite membranes is related to the properties of polymer and nanoparticles as well as chemical interaction between polymer and nanoparticle. Different nanoparticles such as $SiO_2$, $TiO_2$, $Fe_3O_4$, CuO, ZnO, graphene oxide, carbon nanotubes have been incorporated in NF membrane [1,10-14]. Among these nanoparticles, $Fe_3O_4$ NPs have been used in catalysis, smart devices, sensors, drug delivery, and water treatment. The magnetic NPs such as iron oxide NPs are stable at ambient temperature. The magnetic NPs showed excellent reactivity due to presence of hydroxyl groups, ion exchange capacity, and high ability to adsorption. But the recycling of magnetic nanoparticles is difficult. Also, the agglomeration of nanoparticles into the polymeric solutions is high, which reduces its active sites for adsorption pollutant. Some additives such as polyvinylpyrrolidone (PVP) [12], metformin, amine groups [15-17], and carboxymethyl chitosan [18] in the combination with magnetic NPs show the high affinity between membrane and nanoparticles. Coating, immobilization of reactive ligands, and the modification of nanoparticles with polymeric materials and inorganic nanomaterials are various methods for overcoming these challenges [19-23]. Hosseini et al. [12] fabricated hybrid PES/polyvinylpyrrolidone (PVP)-$Fe_3O_4$ NF membranes. These membranes increased pure water flux from 3.14 (L/m$^2$·h) for the pristine membrane to 9.96 (L/m$^2$·h) in 0.1 wt% of PVP-$Fe_3O_4$ NPs. The salt rejection obtained was about 77%-90%. The flux and anti-fouling properties were enhanced compared with the pristine membranes. The flux recover ratio (FRR%) of fabricated membranes was about 69.9% to ~89.5%, while pristine membranes showed FRR% ~46.2%. Zinadini et al. [18] used the carboxymethyl chitosan for the modification of $Fe_3O_4$ NPs. Modified nanoparticles revealed a high flux recovery ratio of about 91.7% at 0.5 wt% NPs. Functionalization of $Fe_3O_4$ NPs by immobilizing silica, metformin, and amine increased the pure water flux and copper ion rejection, which can be explained by nucleophilic functional groups on the surface of the nanoparticle. The highest copper rejection (92%) was obtained for 0.1 wt% metformin-modified silica-coated $Fe_3O_4$ NPs. This modification improved nanoparticle dispersion and more active sites for copper ion adsorption were obtained [15]. Incorporation of aminated $Fe_3O_4$ nanoparticles into the chitosan/polyvinyl alcohol nanofibers was used for NF membrane preparation. The Cr (VI) and Pb (II) rejection achieved 509.7 and 525.8 mg g$^{-1}$, respectively for pH=3 in a binary system, which can be described by electrostatic interaction between protonated amino and hydroxyl groups [24].

Zhu et al. [25] investigated in situ oxidized $Fe_3O_4$ membranes

†To whom correspondence should be addressed.
E-mail: a-moghadassi@araku.ac.ir, s-hosseini@araku.ac.ir

for Cr (VI) and Pb (II) removal with the rejection of about 90% to 100%. Moreover, the use of disodium ethylenediaminetetraacetate dihydrate ($Na_2EDTA$) solution in membrane fabrication improved the adsorption capacity of about 99.75% for Pb (II). Also, high capacity for the elimination of Congo red dye by PVP-coated magnetic NPs ($Fe_3O_4$) was reported by Pandey et al. [26]. The studies showed the significant hydrophilicity and antifouling properties of PES NF membranes by the incorporation of polyaniline modified $Fe_3O_4$ NPs. However, pore blockage occurred in a high concentration of nanoparticles. But membranes showed high separation performance for $Cu^{2+}$ ions [27]. The 8-hydroxyquinoline (8-HQ) is a chelating agent form complex with different metal ions. It has been used to synthesize new material with high potential for the adsorption of pollutants from water [20,28-30]. Nouri et al. [31] reported the surface modification of porous cellulose acetate (CA) membranes by polyvinyl alcohol (PVA)-coated 8-HQ via interfacial polymerization. PVP/$Fe_3O_4$ nanocomposite membranes increased Ni (II) and Cd (II) removal due to creating a complex between metal ions and 8-HQ.

In this study, $Fe_3O_4$ NPs was modified by 8-HQ due to low research studies in the modification of $Fe_3O_4$ NPs by 8-HQ and investigation of their effects in membrane preparation. The different concentrations of modified nanoparticles were used for fabrication of PES-based membranes and investigating separation performance, antifouling properties, and physicochemical properties. The fabricated membranes were characterized by FTIR, FESEM, AFM, and EDX. Contact angle, porosity, mean pore size, pure water flux, and salt rejection and fouling properties were determined for investigation of separation performance by the presence of 8-HQ/$Fe_3O_4$ NPs into the PES as membrane matrix.

## EXPERIMENTAL

### 1. Materials

Polyethersulfone (PES Ultrason E6020P with $M_W$=58,000 g/mol) was purchased from BASF (Germany). PVP as a pore-former agent and N, N-Dimethyl acetamide (DMAc) (87.12 g/mol) as a solvent were purchased from Merck Inc., Germany. 8-hydroxyquinoline (145.16 g/mol), $Fe_3O_4$ NPs (Less than 20 nm) for synthesizing 8-HQ/$Fe_3O_4$ were obtained from Merck Inc., Germany. $MgSO_4$ was provided by Merck Inc., Germany. $MgSO_4$ aqueous solution with a concentration of 1 g/L was used in membrane characterization. All experiments were carried out at pH=7.

### 2. Synthesis of 8-HQ/$Fe_3O_4$ NPs

The modification of $Fe_3O_4$ NPs was performed using 8-HQ according to Kosa et al. [29] method. Briefly, a saturated solution of 8-HQ was prepared in 1,000 mL of deionized water, then stirred for 2 h. The prepared solution was sonicated for 1 h and filtered to remove the undissolved 8-HQ. In the next step, required amounts of $Fe_3O_4$ NPs were added to the saturated solution of 8-HQ and put over a stirrer for 24 h. Modified-$Fe_3O_4$ NPs were separated by filtration and washed with deionized water to remove unreacted 8-HQ. The final products of 8-hydroxyquinoline-$Fe_3O_4$ (8-HQ/$Fe_3O_4$) NPs were dried in an oven at 80 °C during the 24 h.

### 3. Membrane Preparation

The phase inversion process and immersion precipitation were used for the construction of flat sheet NF membranes. The desired amount of PES and PVP (17 : 1 w/w) was dissolved in DMAc under constant stirring for 8 hr. Different concentrations of 8-HQ/$Fe_3O_4$ NPs were added into the solutions in the prior step and were stirred for another 4 h. Then, for better dispersion of nanoparticles, the polymeric solution was sonicated for 30 min. The casting solutions were degassed at room temperature overnight. Then the prepared solutions were cast by an applicator and soaked in the deionized water (DI) for 24 h. The thickness of prepared membranes obtained was 150 μm. The composition detail for prepared membranes is shown in Table 1.

**Table 1. The composition detail of prepared membranes**

| Membrane * | DMAc (wt%) | 8-HQ/$Fe_3O_4$ (wt%) |
|---|---|---|
| M1 | 82.00 | 0.00 |
| M2 | 81.95 | 0.05 |
| M3 | 81.90 | 0.10 |
| M4 | 81.80 | 0.20 |
| M5 | 81.50 | 0.50 |

*PES (17 wt%) and PVP (1 wt%) used as membrane base binder and pore former

### 4. Characterization Methods

Fourier transform Infrared spectroscopy (FTIR, Nicolet 6700) in the range of scanning spectrum 500 to 4,000 $cm^{-1}$ with a resolution of 1 $cm^{-1}$ was used to verify the chemical composition of nanoparticles and their structure.

The size and shape of synthesized nanoparticles and morphology of all prepared membranes were analyzed by field scanning electron microscopy (FSEM) and EDX. Atomic force microscope (AFM) was applied to characterize roughness and surface morphology in a scanning area 6 μm×6 μm.

The overall membrane porosity ($\varepsilon$) and mean pore size of membranes ($r_m$) wer calculated by the following Eq. (1) and (2) [21,32-34] respectively.

$$\varepsilon(\%) = \left(\frac{W_w - W_d}{\rho_f V_m}\right) \times 100 \quad (1)$$

$$r_m = \sqrt{\frac{(2.9 - 1.75\varepsilon) 8 \eta LQ}{\varepsilon A \Delta P}} \quad (2)$$

where $W_w$ (g), $W_d$ (g) are the wet weight and dry weight of membranes. $\rho_f$ (g/$cm^3$) is density.

$V_m$ ($cm^3$) is the volume of the membrane. The water viscosity is $\eta$ ($8.9\times10^{-4}$ Pa·s), Q is the volume rate of permeate pure water flux ($m^3$/s), ΔP, L, A and $\varepsilon$ are operating pressure (0.5 MPa), membrane thickness (m), the area of membrane filtration ($m^2$), respectively. The experiments were repeated three times and the average of results was considered in the evaluation of membrane performance.

Moreover, the water contact angle ($\theta$) was determined by contact angle analyzer and deionized water as probe liquid. The water contact angle ($\theta$) was applied to investigate the hydrophilicity of membranes.

### 5. Membrane Performance Analysis

The separation performance of prepared membranes was ob-

tained by a lab-scale dead filtration set-up with an effective area 11.94 $cm^2$. A schematic diagram of the filtration stirred dead-end cell is shown in Fig. 1. Before taking and analyzing samples, the fabricated membranes were compacted with deionized water at 0.5 MPa for 20 min. Then the filtration test for all prepared membranes was reported with the pressure adjusting in 0.5 MPa. PWF and salts rejection was measured by $J_{w,1}$ (L/$m^2$h), and R (%) via Eqs. (3) and (4).

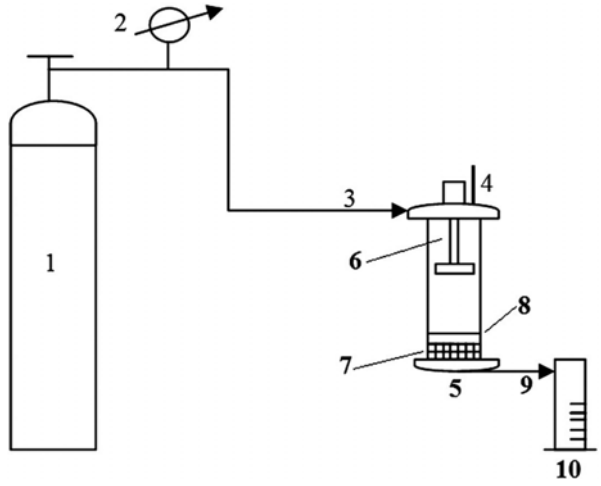


**Fig. 1. Dead-end filtration set-up.**

1. Nitrogen gas
2. Pressure gage
3. Nitrogen entrance
4. Feed entrance
5. Filtration cell
6. Agitator
7. Support
8. Membrane
9. Permeate
10. Collector

$$J_{w,1}=\frac{V}{A\times t} \tag{3}$$

$$R(\%)=\left(1-\frac{C_p}{C_f}\right)\times 100 \tag{4}$$

where V is permeated water volume (*l*), A ($m^2$) is surface area, t is time (h). The feed and permeate ions concentration are $C_f$ and $C_p$, respectively [35,36].

Bovine serum albumin (BSA) aqueous as a fouling agent was used to the characterization of anti-fouling properties at 0.5 MPa for 2 h. Then, the second pure water flux was measured.

## RESULTS AND DISCUSSION

### 1. Characterization of 8-HQ/$Fe_3O_4$ NPs

The synthesized 8-HQ/$Fe_3O_4$ NPs were characterized by FTIR spectra. The FTIR spectra in the rage of 500 to 4,000 $cm^{-1}$ are shown in Fig. 2(a) for 8-HQ, $Fe_3O_4$ NPs, and 8-HQ/$Fe_3O_4$ NPs. All spectra show characteristic peaks of nanoparticles and 8-HQ in the broad of 3,404-3,062 $cm^{-1}$, which are attributed to the stretching

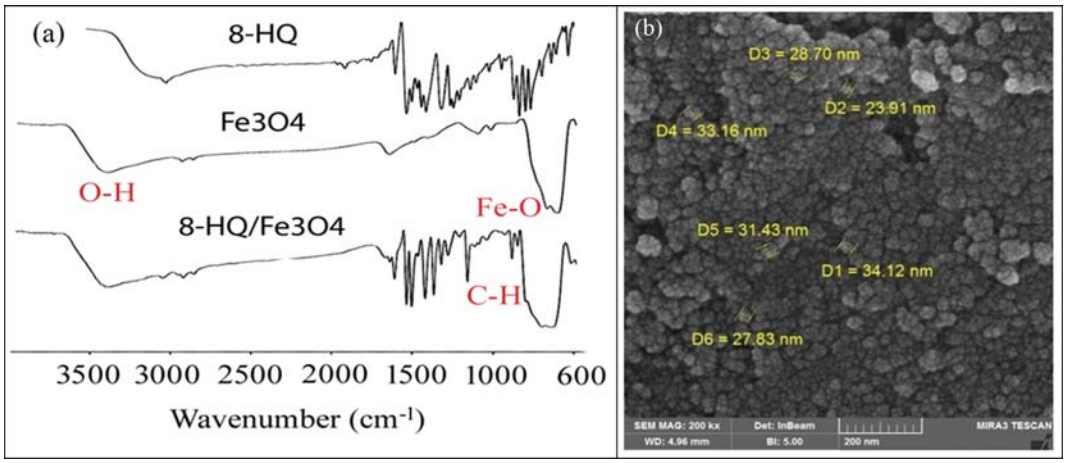


**Fig. 2. (a) FTIR spectra of 8-hydroxyquinoline, $Fe_3O_4$, and 8-HQ/$Fe_3O_4$. (b) FESEM image of 8-HQ/$Fe_3O_4$ nanoparticles.**

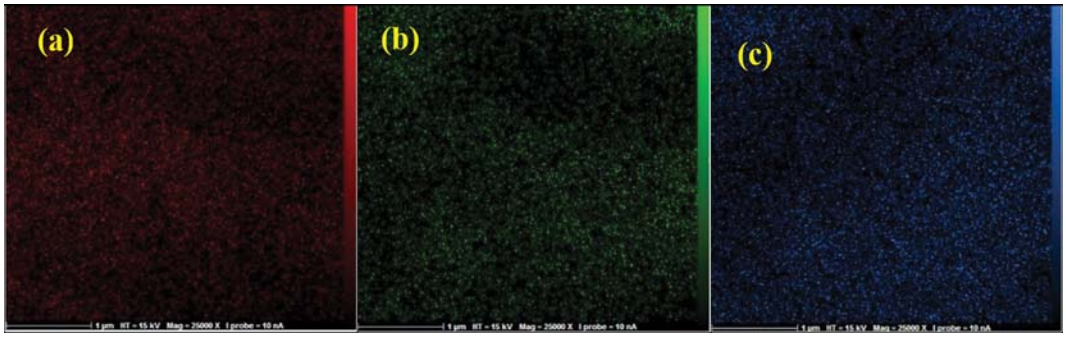


**Fig. 3. EDX mapping of (a) C: carbon, (b) O: oxygen, (c) Fe: Iron for 8-HQ/$Fe_3O_4$ NPs.**

vibration of hydroxy groups in nanoparticles and phenolic hydroxyl groups in 8-HQ with intermolecular interactions. The aromatic amine resonance (C-N-C) is characterized at the peak of 1,275 $cm^{-1}$. The strong peaks in the range of 824 $cm^{-1}$ (region below 1,000 $cm^{-1}$) attributed to the out-of-plane CH wagging vibrations of the quinoline groups. C-C stretching vibration are seen at 1,574 $cm^{-1}$. The displayed bands at 1,497 and 1,464 $cm^{-1}$ may be ascribed to pyridyl and phenyl groups of 8-HQ. Also, absorption peaks at 574 and 631 $cm^{-1}$ show the presence of Fe-O groups in synthesized 8-HQ/$Fe_3O_4$ NPs [37-39]. Fig. 2(b) shows the FESEM images of modified

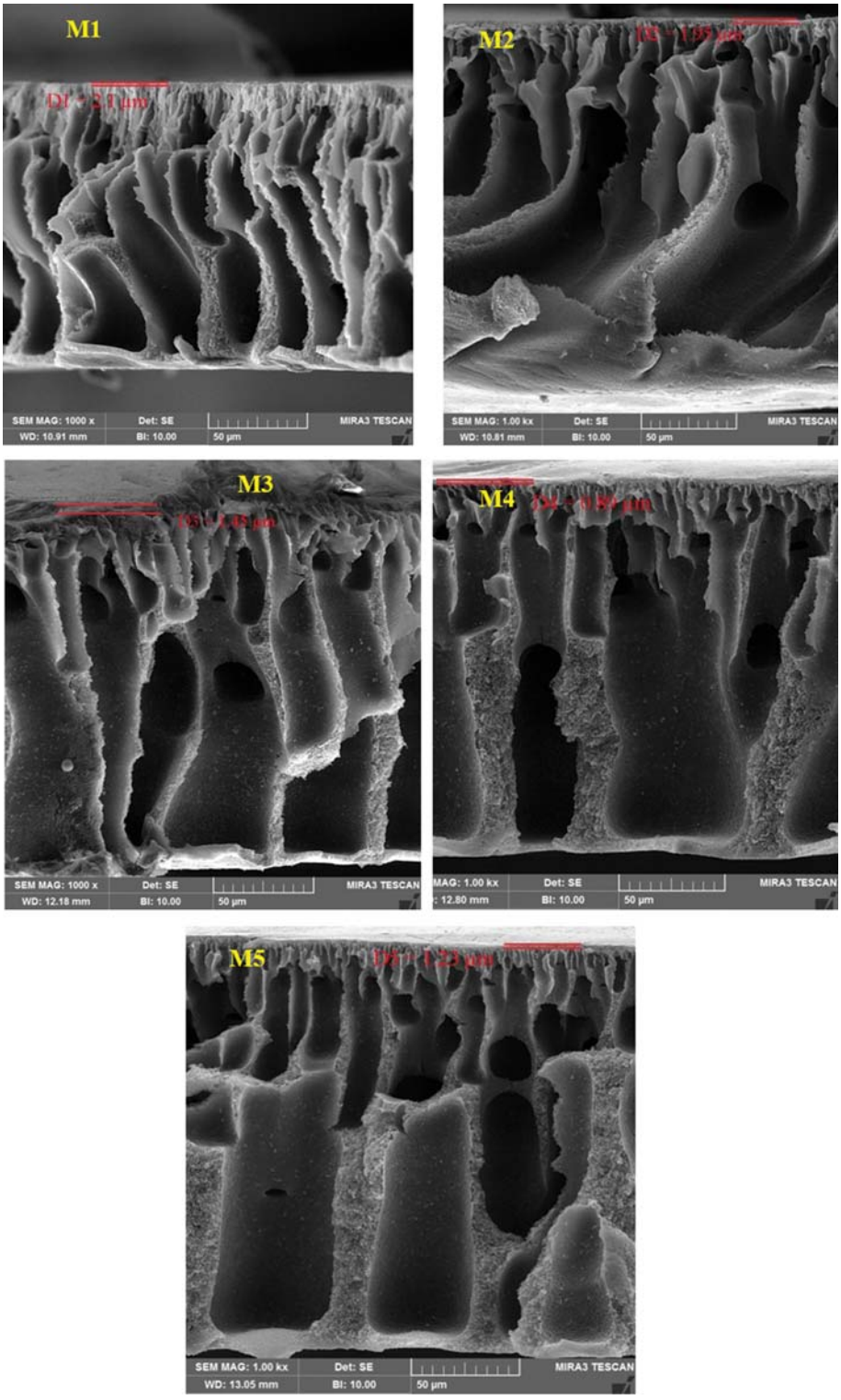


**Fig. 4. Cross sectional FESEM images of the pristine membrane (M1) and modified membranes (M2, M3, M4, M5).**

$Fe_3O_4$ NPs. The average size of nanoparticles obtained was 29.87 nm. The EDX analysis for different elements (carbon, oxygen, and iron) of 8-HQ/$Fe_3O_4$ NPs shown in Fig. 3 confirms the formation of 8-HQ/$Fe_3O_4$ NPs and the presence of C, O, and Fe elements into the structure of 8-HQ/$Fe_3O_4$ NPs.

**2. Characterization of Prepared Membranes**

2-1. Membrane Morphology

FESEM was applied to investigate the morphology of prepared membranes. Fig. 4 shows the cross-sectional FESEM images for the pristine and mixed matrix membranes. All fabricated membranes show an asymmetric structure, including a dense thin top layer and a porous thick sub-layer. The dense layer or selective layer restricts flux and has an important role for the determination of separation performance. Porous layer as membrane supporter has a finger-like structure. The asymmetric structure of fabricated membranes depends on thermodynamic (miscibility) over kinetic (viscosity) effects and the rate of phase inversion process [32,40,41]. Incorporation of 8-HQ/$Fe_3O_4$ NPs as an additive into the membrane structure enhances the membrane hydrophilicity. Therefore, the rate of exchange between solvent and water as non-solvent was enhanced, which its result is more porosities and the formation of channels.

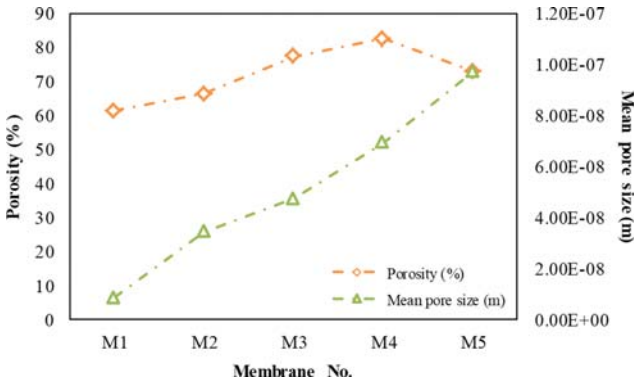


**Fig. 5. Porosity and mean pore size of fabricated membranes.**

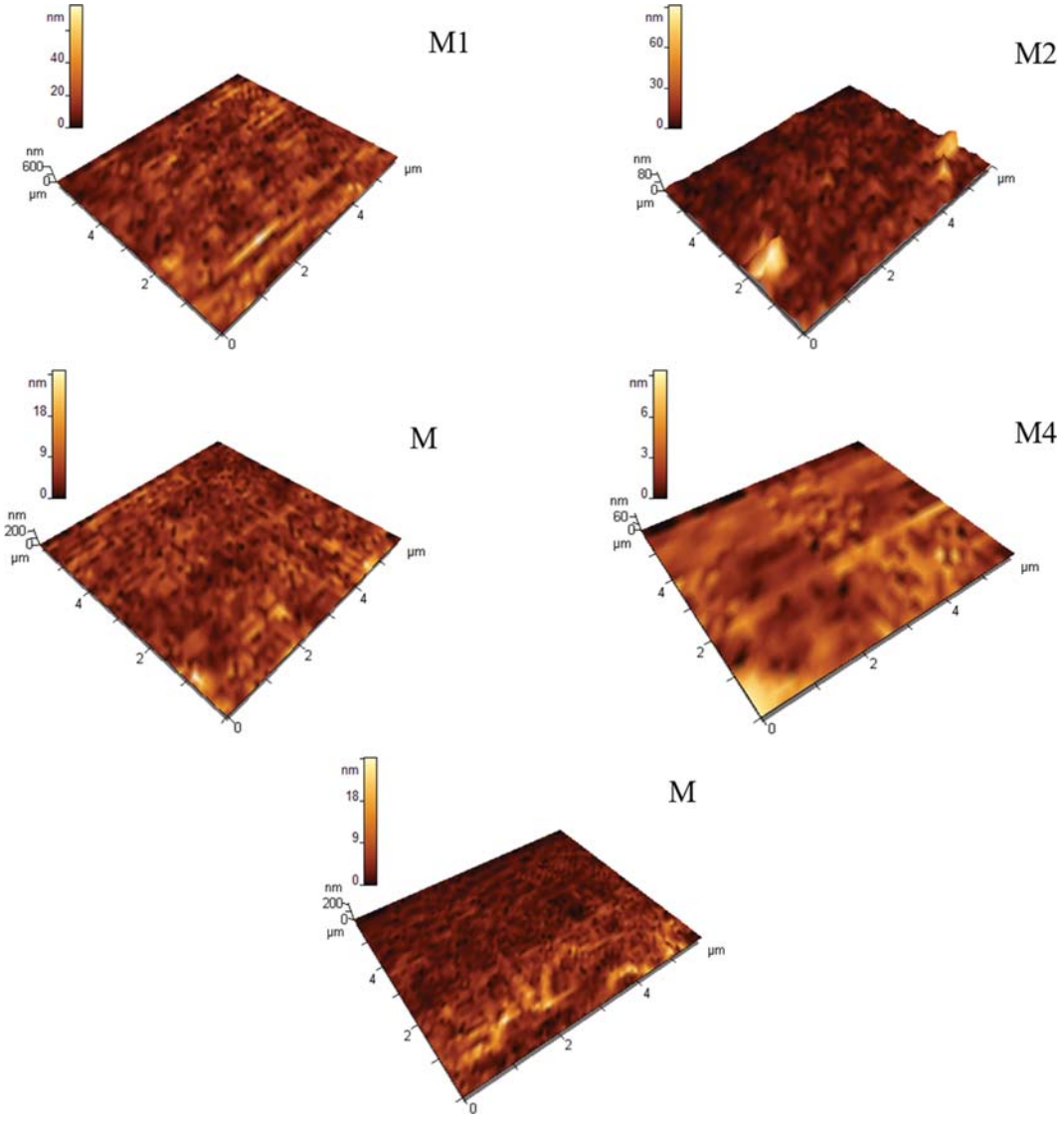


**Fig. 6. Three-dimensional images of AFM for M1-pristine membrane and mixed matrix membranes.**

**Table 2. The parameters of surface roughness for prepared membranes**

| Membrane | $R_a$ (nm) | $R_{max}$ (nm) |
|---|---|---|
| M1 | 5.411 | 33.1 |
| M2 | 4.098 | 19.77 |
| M3 | 1.01 | 5.72 |
| M4 | 1 | 4.601 |
| M5 | 1.472 | 9.677 |

As clear in FESEM images, pristine membrane (M1) shows the small pores into the membrane structure and larger pores are seen for 8-HQ/$Fe_3O_4$ containing membranes. M4 shows more porosity at 0.2 wt% synthesized nanoparticles. However, the small size of pores is clear for M5 in a high concentration of nanoparticles due to increase casting solution viscosity and delayed exchange rate between solvent and non-solvent (water), but it shows the highest thickness of the active layer. Moreover, the nanoparticle migration leads to accumulation on the membrane surface, and the formation of the rougher surface [42,43]. Fig. 5 shows the porosity (%) and mean pore size in pristine and blended membranes. The mean pore size of the membrane was enhanced for mixed matrix membranes (MMMs). The membrane porosity increased from 61.13% for the pristine membrane to 82.4% for M4 in 0.2 wt% 8-HQ/$Fe_3O_4$ NPs. Then, it decreased to 72.85% at 0.5 wt% of 8-HQ/$Fe_3O_4$ NPs, which may be attributed to more casting solution viscosity, the reduction of the mass exchange rate, and pore blockage phenomena by synthesized nanoparticles [44-46].

The surface morphology of prepared membranes was investigated by AFM analysis in the scanning area 6 μm×6 μm, as shown in Fig. 6. The surface roughness of prepared membranes changes by incorporation of synthesized nanoparticles into the PES as membrane matrix. Table 2 shows various roughness parameters in prepared membranes, including average roughness ($R_a$) and the maximum height of roughness ($R_{max}$). Introducing 8-HQ/$Fe_3O_4$ NPs into the membranes was decreased surface roughness of membranes. As shown in Table 2, $R_{max}$ decreases from 33.1 nm for the pristine membrane (M1) to 4.601 nm for 0.2 wt% of nanoparticles due to filling pores with additives and then increases to 9.677 nm for 0.5 wt% 8-HQ/$Fe_3O_4$ NPs. Therefore, modified membranes revealed a smoother surface than the pristine membrane. In a high concentration of 8-HQ/$Fe_3O_4$ NPs for M4 increased $R_{max}$ which can be related to nanoparticle agglomeration on the membrane surface due to the migration of nanoparticles in membrane surface during the phase inversion process [47-49].

2-2. Contact Angle Measurement

One of the most important membrane characteristics that affect membrane performance and antifouling properties is hydrophilicity of the membrane surface. A lower contact angle is indicating more hydrophilicity surface. Therefore, the affinity of water molecules with membrane surface increases by the improvement of membrane hydrophilicity and reduced contact angle [34,50-52]. Fig. 7 shows that by incorporation of 8-HQ/$Fe_3O_4$ NPs in NF membranes, the water contact angle of blended membranes reduced from 68.1° for M1-pristine membrane to 38.3° for M5-0.5 wt% of 8-HQ/$Fe_3O_4$ NPs. The migration of hydrophilic nanoparticles on the membrane surface improved the hydrophilicity of membranes during the phase inversion process. Therefore, the hydrophilicity of modified membranes was enhanced compared to the neat membrane.

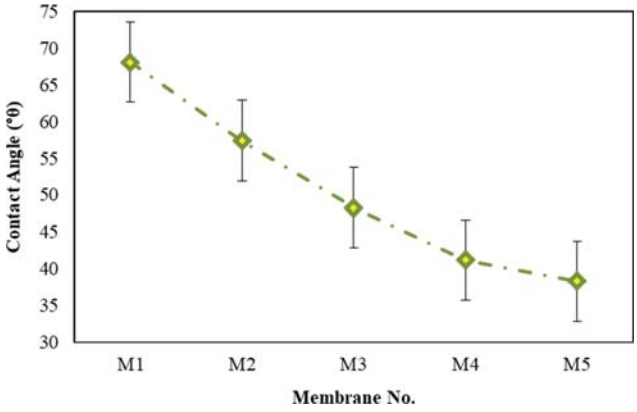


**Fig. 7. Water contact angle of all fabricated membranes.**

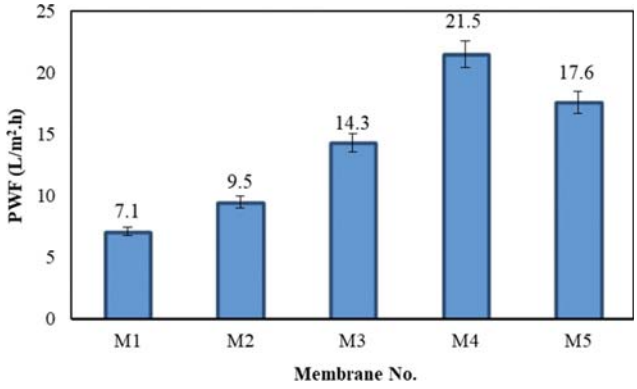


**Fig. 8. Pure water flux of the pristine and mixed matrix membranes at 5 bar.**

2-3. Pure Water Flux

The results of pure water flux are displayed in Fig. 8; that evidences the improvement of PWF by increasing nanoparticles due to more interaction of water molecules with the hydrophilic membrane surface. As shown in Fig. 8, the PWF increased from 7.1 L/$m^2$h in the pristine membrane to 21.5 L/$m^2$h for M4 at 0.2 wt% 8-HQ/$Fe_3O_4$ NPs. For 0.5 wt% of synthesized NPs although declining water contact angle and thus improved membrane hydrophilicity but PWF decreased to 17.6 L/$m^2$h. This contrary behavior is attributed to decreased porosity. Furthermore, nanoparticle agglomeration and pore blockage are other reasons to reduce PWF in a high concentration of 8-HQ/$Fe_3O_4$ NPs [1,21,40,53]. Fig. 9 illustrates a typical FESEM image related to nanoparticle agglomeration and pore blockage at a high concentration of nanoparticles. On the other hand, the formation of the higher thickness of the selective layer in the high concentration of nanoparticles due to high viscosity of casting solution and low phase inversion rate created a barrier for water transport that led to a decline in pure water flux. However, PWF was reduced in a high concentration of 8-HQ/$Fe_3O_4$ NPs, but all modified membranes showed higher PWF than pristine membranes.

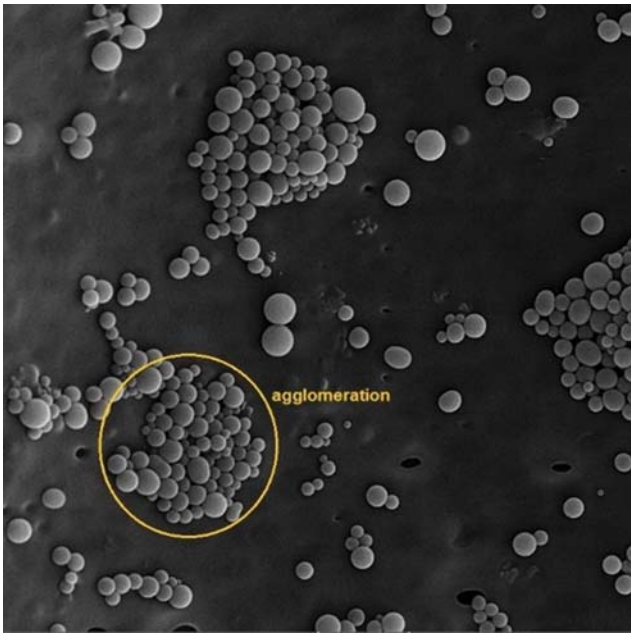


**Fig. 9. The nanoparticle agglomeration or pore blockage at high concentration of 8-HQ/$Fe_3O_4$ NPs on the membrane surface.**

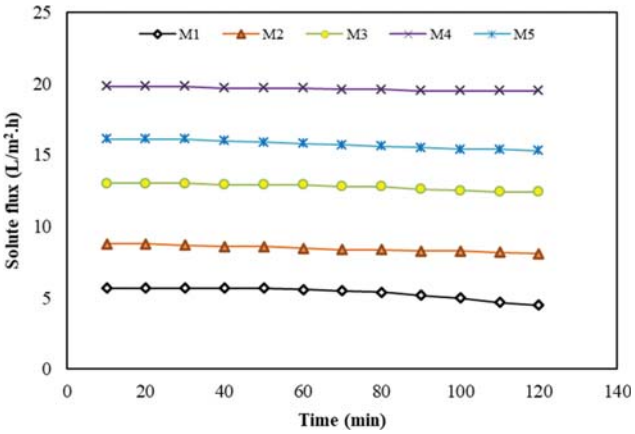


**Fig. 10. Solute flux versus time for the pristine membrane (M1) and mixed matrix membranes (M2, M3, M4, and M5).**

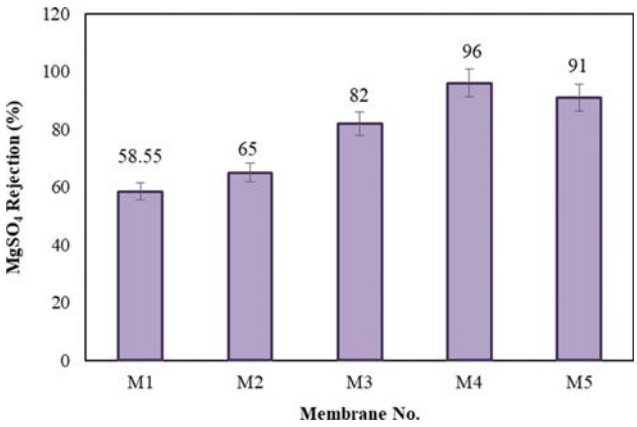


**Fig. 11. Salt rejection of the pristine membrane (M1) and mixed matrix membranes (M2, M3, M4, and M5).**

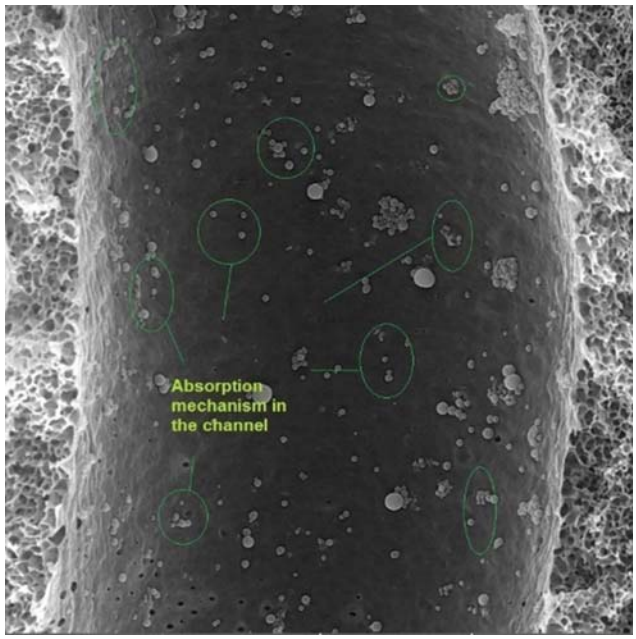


**Fig. 12. The adsorption of salt ions in pores and channels of the modified membrane.**

2-4. Separation Performance

The $MgSO_4$ aqueous solution was used for investigations of filtration performance in MMMs and their comparison with the bare membrane. Fig. 10 shows the change of solute flux in various nanoparticle concentrations versus time. As shown, solute flux enhanced from M1 (pristine membrane) to M4 (0.2 wt% of 8-HQ/$Fe_3O_4$ NPs). The presence of hydrophilic groups such as hydroxyl on the nanoparticle surface would increase the surface hydrophilicity of membranes. Moreover, the uniform dispersion of nanoparticles in a suitable concentration increased the rate of exchange solvent and water during the phase inversion process. According to FESEM images (Fig. 4) and porosity (Fig. 5), the porosity and mean pore size increased by embedding nanoparticles into the PES as membrane matrix and the highest porosity was obtained M4, j, which is in agreement with increasing solute flux and pure water flux. The solute flux decreased in a high concentration of 8-HQ/$Fe_3O_4$ NPs (M5) due to the increase of casting solution viscosity, reduction of porosity, and agglomeration nanoparticles. These items decline the pathways for water molecules transport through the membrane [54,55]. As clear in Fig. 10, all modified membranes showed better separation performance than pristine membrane during the long term.

As shown in Fig. 11, the salt rejection was enhanced by the incorporation of 8-HQ/$Fe_3O_4$ NPs from 58.55% in M1 (pristine membrane) to 96% in M4 (at 0.2 wt% of 8-HQ/$Fe_3O_4$ NPs). The improvement of salt rejection is attributed to the formation of more active sites on the membrane surface that led to high adsorption of salt ions. Fig. 12 shows the absorption of salt ions in pores and channels of the modified membrane. Also, the increasing selective layer thicknesses by introducing nanoparticles increases the resis-

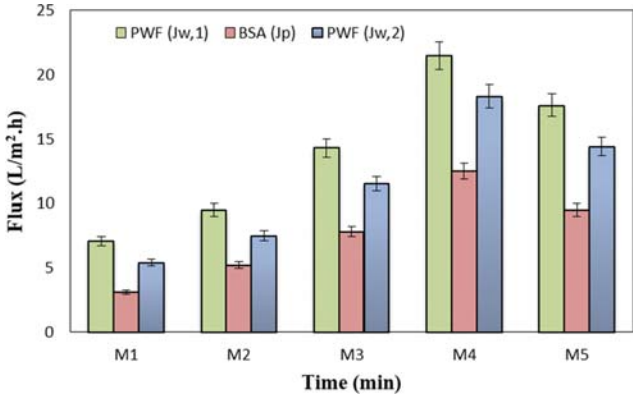


**Fig. 13. Flux versus time for M1 and M4: pure water flux, BSA solution and the pure water flux again.**

tance of membrane against ion transport and thus enhance salt rejection. On the other hand, the presence of negative charge groups, such as hydroxyl on the membrane surface, causes the repulsion of $SO_4^{2-}$ ions and the improvement of salt rejection [56-58]. But at a high concentration of nanoparticles, the rejection decreased to 91% for M5 at 0.5 wt% of 8-HQ/$Fe_3O_4$ due to nanoparticle agglomeration and decreasing active sites on the membrane surface (see Fig. 9).

2-5. Antifouling Properties

The fouling property of NF membranes is one of the greatest challenges in separation performance. The low antifouling properties for the membrane would decrease its flux, selectivity, and long-time stability. In this study, the flux of BSA solution and alternative pure water was used to investigate antifouling properties in fabricated membranes. Fig. 13 shows that M4 at 0.2 wt% of 8-HQ/$Fe_3O_4$ NPs had the best antifouling property due to improving hydrophilic property on the membrane surface.

## CONCLUSION

Hydrophilic 8-HQ/$Fe_3O_4$ NPs were synthesized for the fabrication of mixed matrix membranes. The various concentrations of synthesized nanoparticles were used to investigate the separation performance, physicochemical and antifouling properties of PES-based NF membranes. FTIR, FESEM, and EDX analyses confirmed the synthesis of 8-HQ/$Fe_3O_4$ NPs. FESEM images showed an asymmetric structure of NF membranes. AFM showed the smoother surface of membranes in various concentrations of nanoparticles compared to the pristine membrane. Porosity and mean pore size of modified membranes improved compared with the bare membrane. M4 at 0.2 wt% nanoparticles showed the highest pure water flux (21.5 L/$m^2$h), while it was 7.1 L/$m^2$h for the pristine membrane. Moreover, the salt rejection improved from 58.55% in M1 (pristine membrane) to 96% in M4 (at 0.2 wt% of 8-HQ/$Fe_3O_4$ NPs). The modified membranes showed suitable antifouling property.

## ACKNOWLEDGEMENT

Authors gratefully acknowledge Arak University for the financial support during this study.

## REFERENCES

1. E. Bagheripour, A. Moghadassi, S. Hosseini, B. Van der Bruggen and F. Parvizian, *J. Ind. Eng. Chem.*, **62**, 311 (2018).
2. S. Ansari, A. R. Moghadassi and S. M. Hosseini, *Desalination*, **357**, 189 (2015).
3. M. Maarefian, S. Bandehali, S. Azami, H. Sanaeepur and A. Moghadassi, *Int. J. Energy Res.*, **43**, 8217 (2019).
4. H. Sanaeepur, A. E. Amooghin, S. Bandehali, A. Moghadassi, T. Matsuura and B. van der Bruggen, *Prog. Polym. Sci.*, **91**, 80 (2019).
5. S. Bandehali, H. Sanaeepur, A. Ebadi Amooghin and A. R. Moghadassi, in *Modeling in membranes and membrane-based processes*, A. Roy, S. Moulik, R. Kamesh, A. Mullick Eds., Wiley & Sons, Inc., Hoboken (2020).
6. S. M. Hosseini, F. Karami, S. K. Farahani, S. Bandehali, J. Shen and E. Bagheripour, *Korean J. Chem. Eng.*, **37**, 866 (2020).
7. T. S. Jamil, E. S. Mansor, H. Abdallah, A. M. Shaban and E. R. Souaya, *J. Environ. Chem. Eng.*, **6**, 3273 (2018).
8. S. Bandehali, A. Kargari, A. Moghadassi, H. Saneepur and D. Ghanbari, *ASIA-PAC J. Chem. Eng.*, **9**, 638 (2014).
9. H. Sanaeepur, A. Ebadi Amooghin and S. Bandehali, *Theoretical gas permeation models for mixed matrix membranes*, LAP LAMBERT Academic Publishing, Beau Bassin, Mauritius (2018).
10. N. Rakhshan and M. Pakizeh, *J. Ind. Eng. Chem.*, **34**, 51 (2016).
11. A. Azari, R. Rezaei and H. Sanaeepur, *Desalin. Water. Treat.*, **124**, 308 (2018).
12. S. M. Hosseini, M. Afshari, A. R. Fazlali, S. Koudzari Farahani, S. Bandehali, B. van der Bruggen and E. Bagheripour, *Chem. Eng. Res. Des.*, **147**, 390 (2019).
13. Y. T. Chung, E. Mahmoudi, A. W. Mohammad, A. Benamor, D. Johnson and N. Hilal, *Desalination*, **402**, 123 (2017).
14. H.-Z. Zhang, Z.-L. Xu and J.-Y. Sun, *RSC Adv.*, **8**, 29455 (2018).
15. N. Ghaemi, S. S. Madaeni, P. Daraei, H. Rajabi, S. Zinadini, A. Alizadeh, R. Heydari, M. Beygzadeh and S. Ghouzivand, *Chem. Eng. J.*, **263**, 101 (2015).
16. B. R. White, B. T. Stackhouse and J. A. Holcombe, *J. Hazard. Mater.*, **161**, 848 (2009).
17. S. Azari and L. Zou, *Desalination*, **324**, 79 (2013).
18. S. Zinadini, A. Zinatizadeh, M. Rahimi, V. Vatanpour, H. Zangeneh and M. Beygzadeh, *Desalination*, **349**, 145 (2014).
19. H. Zangeneh, A. A. Zinatizadeh, S. Zinadini, M. Feyzi and D. W. Bahnemann, *React. Funct. Polym.*, **127**, 139 (2018).
20. N. Abdali, A. Marjani, F. Heidary and M. Adimi, *New J. Chem.*, **41**, 6405 (2017).
21. A. Gholami, A. Moghadassi, S. Hosseini, S. Shabani and F. Gholami, *J. Ind. Eng. Chem.*, **20**, 1517 (2014).
22. A. R. Moghadassi, E. Bagheripour and S. M. Hosseini, *J. Appl. Polym. Sci.*, **134**, 44993 (2017).
23. F. Javaheri and S. Hassanajili, *J. Appl. Polym. Sci.*, **133**, 44330 (2016).
24. S. Koushkbaghi, A. Zakialamdari, M. Pishnamazi, H. F. Ramandi, M. Aliabadi and M. Irani, *Chem. Eng. J.*, **337**, 169 (2018).
25. M. Zhu, L. Zhu, J. Wang, T. Yue, R. Li and Z. Li, *J. Environ. Manage.*, **196**, 127 (2017).
26. G. Pandey, S. Singh and G. Hitkari, *Int. Nano Lett.*, **8**, 111 (2018).
27. P. Daraei, S. S. Madaeni, N. Ghaemi, E. Salehi, M. A. Khadivi, R. Moradian and B. Astinchap, *J. Membr. Sci.*, **415**, 250 (2012).

28. C. Liu, X. Sun, L. Liu, J. Liu, M. Qi and H. An, *Desalin Water Treat.*, **57**, 18425 (2016).
29. S. A. Kosa, G. Al-Zhrani and M. Abdel Salam, *Chem. Eng. J.*, **181-182**, 159 (2012).
30. Y. Li, B. Gao and X. Fang, *J. Chem. Technol. Biotechnol.*, **88**, 1459 (2013).
31. M. Nouri, A. Marjani, M. Tajdari, F. Heidary and M. Salimi, *Colloid Polym. Sci.*, **296**, 1213 (2018).
32. E. Bagheripour, A. Moghadassi and S. M. Hosseini, *Korean J. Chem. Eng.*, **33**, 1462 (2016).
33. A. Rahimpour, *Desalination*, **265**, 93 (2011).
34. P. Mobarakabad, A. Moghadassi and S. Hosseini, *Desalination*, **365**, 227 (2015).
35. E. Bagheripour, A. Moghadassi and S. Hosseini, *Int. J. Eng. Sci.*, **33**, 1462 (2016).
36. S. Hosseini, E. Bagheripour, A. Hamidi, A. Moghadassi and S. Madaeni, *J. Iran Chem. Soc.*, **13**, 1749 (2016).
37. V. B. Devi, P. Arulmozhichelvan and P. Murugakoothan, *Bull. Mater. Sci.*, **40**, 1049 (2017).
38. Z. Shahedi, M. R. Jafari and A. A. Zolanvari, *J. Mater. Sci.: Mater. Electron.*, **28**, 7313 (2017).
39. S. Rostamnia, B. Gholipour, X. Liu, Y. Wang and H. Arandiyan, *J. Colloid Interface Sci.*, **511**, 447 (2018).
40. E. Bagheripour, A. Moghadassi and S. M. Hosseini, *Int. J. Eng. Sci.*, **30**, 821 (2017).
41. D. Emadzadeh, W. J. Lau, T. Matsuura, M. Rahbari-Sisakht and A. F. Ismail, *Chem. Eng. J.*, **237**, 70 (2014).
42. S. Bandehali, A. Moghadassi, F. Parvizian, Y. Zhang, S. M. Hosseini and J. Shen, *Sep. Purif. Technol.*, **242**, 116745 (2020).
43. F. Parvizian, F. Ansari and S. Bandehali, *Chem. Eng. Res. Des.*, **156**, 433 (2020).
44. S. Bandehali, F. Parvizian, A. Moghadassi and S. M. Hosseini, *Sep. Purif. Technol.*, **237**, 116361 (2019).
45. S. Bandehali, F. Parvizian, A. R. Moghadassi and S. M. Hosseini, *J. Polym. Res.*, **26**, 211 (2019).
46. S. Bandehali, F. Parvizian, A. R. Moghadassi, S. M. Hosseini and J. N. Shen, *J. Polym. Res.*, **27**, 94 (2020).
47. S. Bandehali, A. Moghadassi, F. Parvizian and S. Hosseini, *Korean J. Chem. Eng.*, **36**, 1657 (2019).
48. S. Bandehali, A. Moghadassi, F. Parvizian, S. M. Hosseini, T. Matsuura and E. Joudaki, *J. Energy Chem.*, **46**, 30 (2020).
49. S. Bandehali, A. Moghadassi, F. Parvizian, J. Shen and S. Hosseini, *Korean J. Chem. Eng.*, **37**, 263 (2020).
50. S. Ansari, E. Bagheripour, A. Moghadassi and S. M. Hosseini, *J. Polym. Eng.*, **37**, 61 (2017).
51. S. M. Hosseini, P. Koranian, A. Gholami, S. S. Madaeni, A. R. Moghadassi, P. Sakinejad and A. R. Khodabakhshi, *Desalination*, **329**, 62 (2013).
52. S. M. Hosseini, A. Hamidi, A. Moghadassi and S. S. Madaeni, *Korean J. Chem. Eng.*, **32**, 429 (2015).
53. E. Bagheripour, A. Moghadassi, S. Hosseini, M. Ray, F. Parvizian and B. van der Bruggen, *Chem. Eng. Res. Des.*, **132**, 812 (2018).
54. S. Hosseini, E. Jashni, M. Jafari, B. Van der Bruggen and Z. Shahedi, *J. Membr. Sci.*, **560**, 1 (2018).
55. A. Moghadassi, E. Bagheripour, F. Parvizian and S. Hosseini, *Int. J. Eng. Sci.*, **31**, 1609 (2018).
56. R. W. Baker, *Membrane technology and applications*, 3th Ed., Wiley, United Kingdom (2012).
57. B. Van der Bruggen, C. Vandecasteele, T. Van Gestel, W. Doyen and R. Leysen, *Environ. Prog.*, **22**, 46 (2003).
58. H. Zhang, B. Li, J. Pan, Y. Qi, J. Shen, C. Gao and B. Van der Bruggen, *J. Membr. Sci.*, **539**, 128 (2017).